

Effects of Temperature on Particle Coalescence in the Selective Laser Sintering Process

Cheung, See Lin; Chua, Chee Kai; Zhou, Kun; Wei, Jun

2014

Cheung, S. L., Chua, C. K., Zhou, K., & Wei, J. (2014). Effects of Temperature on Particle Coalescence in the Selective Laser Sintering Process. Proceedings of the 1st International Conference on Progress in Additive Manufacturing (Pro-AM 2014), 24-29.

<https://hdl.handle.net/10356/84375>

https://doi.org/10.3850/978-981-09-0446-3_096

© 2014 by Research Publishing Services.

Downloaded on 13 Mar 2024 16:53:24 SGT

EFFECTS OF TEMPERATURE ON PARTICLE COALESCENCE IN THE SELECTIVE LASER SINTERING PROCESS

SEE LIN CHEUNG ^{1,2}, CHEE KAI CHUA ^{1,3*}, KUN ZHOU ^{1,3,*}, JUN WEI ^{1,2}

¹ SIMTech-NTU Joint Laboratory (3D Additive Manufacturing), Nanyang Technological University, 50 Nanyang Avenue, Singapore 639798

² Singapore Institute of Manufacturing Technology, 71 Nanyang Drive, Singapore 638075

³ NTU Additive Manufacturing Centre, School of Mechanical & Aerospace Engineering, Nanyang Technological University, 50 Nanyang Avenue, Singapore 639798, Singapore

ABSTRACT: The interaction between powder particles during laser irradiation is one of the major factors affecting the build part in the selective laser sintering process. Due to asymmetric heating, defects such as internal voids, disjoint particles and asymmetrical shrinkages are formed within the part. This paper utilizes molecular dynamics simulation to reveal the effects of asymmetric heating on the build part.

INTRODUCTION

Selective laser sintering (SLS) is an additive manufacturing process where the part is built up layer by layer through the joining of powder particles by laser irradiation. As the powder particles are irradiated, they experience a spike in temperature followed by rapid cooling back to the temperature of the chamber which holds these particles. Depending on the materials used, laser power and chamber temperature may vary, with metals typically having a higher temperature as compared to polymers.

Besides the laser power and chamber temperature, there are many other parameters to consider during the SLS process, including scan speed, scan strategies, powder size and build orientation. To determine a working set of parameters, trial parts often have to be built and iterated which results in much wastage especially when a new material is introduced. Conducting the iterative methods using a computer model to determine the initial set of parameters is therefore ideal as the material cost of building the trial parts can be saved.

The SLS process is similar to the sintering process proposed by Frenkel (1945) who established an analytical model to predict the evolution of the two-particle sintering over time. The model was then improved by Pokluda et al. (1997) and subsequently further developed by Bellehumeur et al. (1998) and Scribben et al. (2006) which included the effects of viscoelasticity. Some other approaches have also been adopted to model the sintering process. Kolossov et al. (2004) conducted an FEM analysis on a cube-shaped part and simulated the temperature distribution over the surface. MD study of the two particle sintering process has also been conducted by Zhu et al. (1996), Yang et al. (2012), and Wang (2010) showing the time evolution of a two particle system.

In this paper, MD simulations are conducted to study the sintering process of gold particles during which an exponential cooling model is adopted. A one-dimensional model is built by lining up a series of two particles and heating them up at different time intervals. Much work has been carried out for gold atoms by Yang et al. (2012) and Wang (2010), which serve as the basis of this study.

* Corresponding Authors.

Email addresses: mckchua@ntu.edu.sg (C. K. Chua), kzhou@ntu.edu.sg (K. Zhou).

SIMULATION PROCEDURES

The MD simulations in this work are conducted using the Large-scale Atomic/Molecular Massively Parallel Simulator (LAMMPS) by Plimpton (1995). Spherical gold particles are created with FCC crystal structure for all the particles. A lattice constant of 4.08 Å is used and the particles are placed 1 Å apart from each other. The particle diameter is approximately 6.5 nm which is the width of 16 atoms. The mass of the atoms are set at 196.97 Da. Two pair potentials are investigated in the simulation procedures. The first is the Morse potential and the second is the Embedded Atom Method (EAM) potential. The constants used for the Morse model are obtained from Kozlov et al. (1972), while the EAM model uses values from Grochola et al. (2005) obtained from the National Institute of Standards and Technology.

The assumptions made for the simulations are as follows:

- The entire particle is heated up to the same temperature instantaneously.
- Conduction and radiative heat transfer is relatively small compared to convection cooling and thus is ignored.
- The change in surface area of the particles does not significantly affect the cooling rate.
- The particles are immersed in a bath of inert gas which removes heat from the particles but has negligible interactions with the particles.

The temperature T for each particle is assumed to be exponentially decreasing over time for convective cooling following:

$$T = Ae^{-\frac{t}{\tau}} + T_{\infty}, \quad (3)$$

$$T_f = 0.02A + T_{\infty}, \quad (4)$$

where τ is a time constant, $A + T_{\infty}$ is the temperature at $t = 0$, and T_f is the temperature at $t = t_f$. The temperature is assumed to have reached steady state once it reaches 98 % of the value. The initial values of T is chosen to be at 2800 K and the steady state temperature is chosen to be at 800 K. For the temperature to decay fully from 2800 K to 800 K at 100 ps, τ is determined to be 25.6 ps while for a decay time of 300 ps, τ is determined to be 76.7 ps. Output results are taken at 0.5 ps intervals. The setup is as shown in Figure 1:

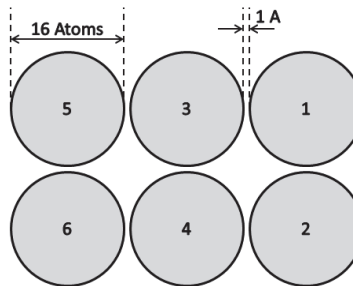


Figure 1. Configuration of simulation setup. The circles represent spheres made up of atoms with 16 atoms diameter FCC crystal structure with 1 Å separation.

We will first be looking at the effects of the case where the particles are all heated up together with the Morse potential utilizing run parameters: constant temperature at 2800 K for a baseline run; $\tau = 25.6$ ps for the second run; and $\tau = 76.7$ ps for the third run. We will then be looking to compare the effects of the pair potentials EAM and Morse; together with the effects of $\tau = 25.6$ ps and $\tau = 76.7$ ps; and the time difference between the heating of particles at 15 ps and 30 ps. A baseline run is also carried out for each of the parameters where the temperature is held at 2800 K.

The time steps used in the simulation was 1 fs and a microcanonical ensemble (NVE), together with Langevin thermostat is used to simulate the removal of heat through a bath as described by Grønbech-Jensen et al. (2013). An initial energy minimization run was setup to ensure that the particles start in a relaxed state. The notations defined in this paper to describe the particles will be p_i for particle i, g_A for group 1 which consists of p_1 and p_2 , g_B for group 2 which consists of p_3

and p_4 , g_C for group 3 which consists of p_5 and p_6 . τ is defined as $\tau_1 = 25.6$ ps, $\tau_2 = 76.7$ ps. The time difference between heating of g_A , g_B , g_C is denoted as Δ_{15} for 15 ps time interval and Δ_{30} for 30 ps time interval.

RESULTS AND DISCUSSION

From Figure 2, it is observed that for the case with same heating time, the voids between the particles do not close in both the simulations using τ_1 and τ_2 , but in the case of the baseline run it fully closes. The particle coalescence is also observed to stop at about 1400 K which is approximately the melting point of gold. It is also observed that the longer the heating rate, the more coalescence occurs between particles. Shrinkages are also observed as the particles coalesce together to fill up the voids.

From Figure 3 and 4, the particles behave similarly in the first 10 ps for both the Morse and the EAM potentials with different heating times. Necking first forms between p_1 and p_2 , followed by p_1 and p_3 , and p_2 and p_4 , with g_B moving towards g_A . This causes g_B to move away from g_C and there is a threshold distance whereby no interaction occurs between p_3 and p_5 , and p_4 and p_6 . This would result in two separate particles being formed with no joining between them as in many of the cases.

In some cases, as in the baseline Δ_{30} in the Morse potential, a secondary neck is formed long after the particles are joined together. This occurs as the particles coalesce, they approach that of a spherical form as it has the least surface energy. This causes the width of the particles to expand while the height decreases resulting in the particles approaching each other once again which leads to neck growth between the two spheroids as seen in Figure 3(g). It is also observed that due to the asymmetric heating of the particles, the voids close in at different rates and are different in size at the end of simulation where the particle freezes. This therefore implies that a larger difference in starting time between g_A and g_B will lead to more coalescence between direct neighboring particles but may lead to no interactions with further particles.

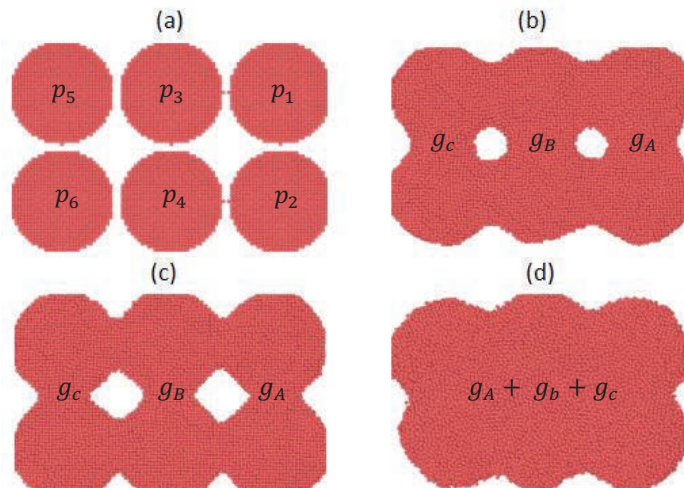


Figure 2. Simulation results for same heating time. (a) Initial configuration of simulation. (b) End of simulation using τ_1 at 192 ps. (c) End of simulation using τ_2 at 100 ps. (d) End of simulation at 192 ps baseline run.

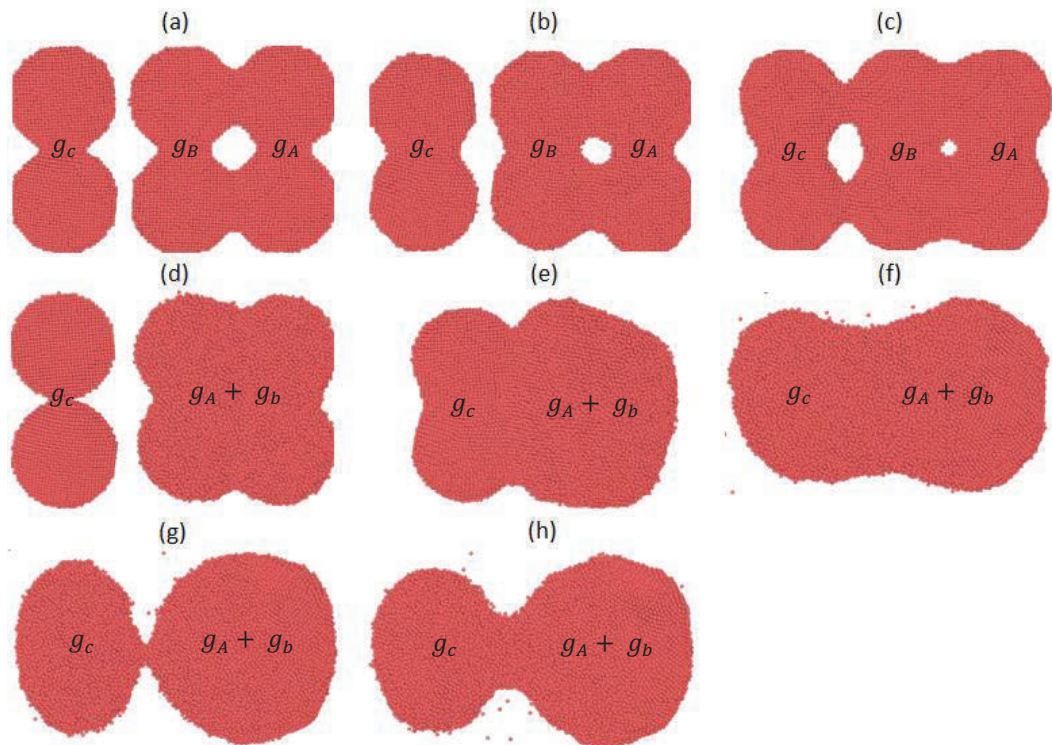


Figure 3. Configurations of the particles under different run parameters at different times as labelled. (a) τ_1 and Δ_{15} at 130 ps. (b) τ_1 and Δ_{30} at 160 ps. (c) τ_2 and Δ_{15} at 330 ps. (d) τ_2 and Δ_{30} at 64 ps. (e) τ_2 and Δ_{30} at 308 ps. (f) Baseline Δ_{15} at 330 ps. (g) Baseline Δ_{30} at 322 ps. (h) Baseline Δ_{30} at 360 ps.

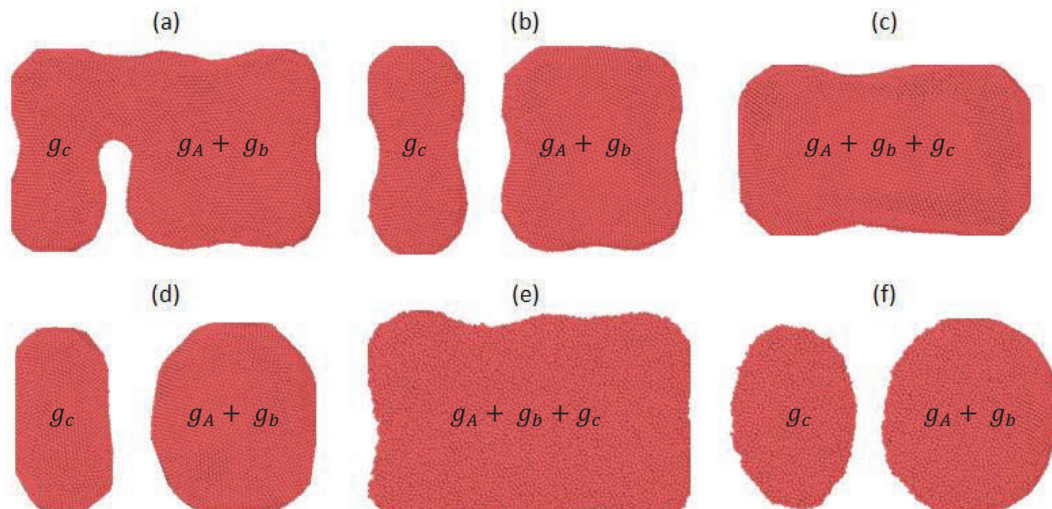


Figure 4. Configurations of the particles under different run parameters at different times as labelled. (a) τ_1 and Δ_{15} at 130 ps. (b) τ_1 and Δ_{30} at 160 ps. (c) τ_2 and Δ_{15} at 330 ps. (d) τ_2 and Δ_{30} at 360 ps. (e) Baseline Δ_{15} at 330 ps. (f) Baseline Δ_{30} at 360 ps.

CONCLUSION

It is found that a fast cooling rate leads to a smaller neck radius and internal voids are formed due to the particles freezing. Meanwhile, a slow cooling rate leads to improved coalescence between the particles but causes the particle size to shrink, in some cases leading to no fusion between neighboring particles. Also, a lower time difference between heating of g_1 and g_2 leads to better joining between the particles, while the reverse case allows for better coalescence but might lead to no fusion between neighboring particles. This is an interesting phenomenon as it indicates that a compromise might be required between internal voids or complete joining of the structure. The particles were also observed to freeze at around 1400 K which is approximately the melting point of gold. Shrinkages were also observed in the simulation as the atoms rearrange to fill in the voids resulting in a denser part.

The next goal of the model development is to apply coarse grain methods to scale up to the nanometer range to get a better understanding of the SLS process as the powder particles used are in the range of 50-100 nm. Other elements and polymers compounds can then be used as the grains to simulate the effects of different materials in order to obtain a set of initial working parameters which will result in less wastage of materials building the trial parts.

ACKNOWLEDGEMENTS

This work is supported by the Agency for Science, Technology and Research, Singapore through the Industrial Additive Manufacturing Program (SERC Grant No: 132 550 4106).

REFERENCES

- Bellehumeur, C. T., Kontopoulou, M., & Vlachopoulos, J. (1998). The role of viscoelasticity in polymer sintering. *Rheologica Acta*, 37(3), 270-278
- Frenkel, J. (1945). Viscous Flow of Crystalline Bodies under the Action of Surface Tension. *Journal of Physics USSR*(9), 385-391
- Grochola, G., Russo, S. P., & Snook, I. K. (2005). On fitting a gold embedded atom method potential using the force matching method. *The Journal of Chemical Physics*, 123(20), -
- Grønbech-Jensen, N., & Farago, O. (2013). A simple and effective Verlet-type algorithm for simulating Langevin dynamics. *Molecular Physics*, 111(8), 983-991
- Kolossov, S., Boillat, E., Glardon, R., Fischer, P., & Locher, M. (2004). 3D FE simulation for temperature evolution in the selective laser sintering process. *International Journal of Machine Tools & Manufacture*, 44(2-3), 117-123
- Kozlov, É. V., Popov, L. E., & Starostenkov, M. D. (1972). Calculation of the morse potential for solid gold. *Soviet Physics Journal*, 15(3), 395-396
- Plimpton, S. (1995). Fast Parallel Algorithms for Short-Range Molecular Dynamics. *Journal of Computational Physics*, 117(1), 1-19
- Pokluda, O., Bellehumeur, C. T., & Vlachopoulos, J. (1997). Modification of Frenkel's model for sintering. *AIChE Journal*, 43(12), 3253-3256
- Scribben, E., Baird, D., & Wapperom, P. (2006). The role of transient rheology in polymeric sintering. *Rheologica Acta*, 45(6), 825-839
- Wang, N. (2010). *Melting, solidification and sintering/coalescence of nanoparticles*
- Yang, L. Q., Gan, Y., Zhang, Y. W., & Chen, J. K. (2012). Molecular dynamics simulation of neck growth in laser sintering of different-sized gold nanoparticles under different heating rates. *Applied Physics a-Materials Science & Processing*, 106(3), 725-735
- Zhu, H. L., & Averback, R. S. (1996). Sintering processes of two nanoparticles: A study by molecular-dynamics. *Philosophical Magazine Letters*, 73(1), 27-33